*American Mineralogist, Volume 98, pages 927–931, 2013*

# Kinking in $Mg_2GeO_4$ olivine: An EBSD study† 🔓

**Pamela C. Burnley,* Christopher J. Cline II, and Alex Drue**

Department of Geosciences and High Pressure Science and Engineering Center, University of Nevada, Las Vegas, Nevada 89154-4010, U.S.A.

## Abstract

We have used electron backscatter diffraction (EBSD) to characterize the internal deformation and orientation of olivine grains within an experimentally deformed $Mg_2GeO_4$ olivine aggregate. We observe that a significant fraction of the grains contain kink bands. Our observations of kink band geometry, combined with the work of earlier authors, indicate that [001] slip is the dominant slip system operating in $Mg_2GeO_4$ olivine at 1000–1473 K at 0.6–1.3 GPa. Since $Mg_2GeO_4$ is a high-pressure analog for natural compositions of olivine, this is consistent with the observations made by others that the dominant slip system for olivine in the mantle switches from [100] to [001] as pressure increases. We also observed that kink bands formed in all measured olivine grains with [001] axes oriented within 35° of the compression direction. We thus conclude that in a randomly oriented polycrystal undergoing uniaxial deformation at low to moderate temperatures, 18% of all grains will deform by kinking and that kink band formation is an important accommodation mechanism for olivine at these conditions.

**Keywords:** Olivine, deformation, kink band, electron backscatter diffraction

## Introduction

The rheological properties of olivine are widely believed to control flow in the upper mantle and have therefore been the subject of extensive research for the last 50 years. An interesting facet of plastic deformation of olivine is that its slip systems do not satisfy the von Mises criterion for arbitrary shape change. There are eight slip systems commonly observed to operate in olivine [for review see Cordier et al. (2002)]. However, many of them are linear combinations of others yielding only three truly independent slip systems [for discussion see Durham and Goetze (1977); Castelnau et al. (2010)]. Olivine polycrystals overcome this failure to meet the von Mises criteria, in part, by kinking. Kinking is interpreted to result from a buckling instability that occurs when planes of weakness (in this case easy glide directions) are oriented parallel to compression (Raleigh 1968). Kinking is commonly observed in olivine deformed at low to moderate temperatures both experimentally and naturally (e.g., Raleigh 1968; Mercier and Nicolas 1975; Durham and Goetze 1977; Zeuch and Green 1984a, 1984b; Ave Lallemant 1985; Kopylova et al. 1999; Bjerg et al. 2005; Chernyshov 2005; Low et al. 2011). Kinking received substantial attention in early deformation studies (e.g., Raleigh 1968) in part because measurements of the kink band geometry allow the slip direction and slip plane to be determined. More recent rheological studies have focused on characterizing the behavior of grains oriented for slip and avoided the strain heterogeneity associated with kinking. However, to model the deformation of polycrystalline olivine, for example using viscoplastic or elastic plastic self-consistent models, a full description of the deformation and accommodation mechanisms is required.

To understand the role of kinking in olivine deformation we characterized individual kinked grains using electron backscatter diffraction (EBSD). To our knowledge, this has not been done for olivine. We choose to study kinking in experimentally deformed $Mg_2GeO_4$ because we had samples with a fairly coarse grain size on hand (Burnley 1990).

## Methods

This study was conducted on experimentally deformed polycrystalline $Mg_2GeO_4$. Details of the sample synthesis, preparation, and deformation experiments can be found in (Burnley et al. 1991; Burnley 1990). Conditions for the deformation experiments are listed in Table 1. It should be noted that at these pressure temperature conditions, the olivine phase of $Mg_2GeO_4$ is metastable with respect to the cubic spinel structured polymorph (Ross and Navrotsky 1987). Thin sections of the samples, prepared in the plane of the thermocouple, were polished to a 1 µm finish and then polished with a 0.05 µm colloidal silica slurry on a vibratory polisher for 4 h. The samples were examined using an Oxford Nordlys II EBSD detector on a JEOL JSM-5610 scanning electron microscope. Orientation image maps were collected at accelerating voltages of 15 and 20 keV, with a Hough resolution between 55 and 100, and using between 5 and 8 bands for phase detection. The highest indexing rates (60%) were observed at 20 keV, with a Hough resolution of 80 and using 6–7 bands for phase detection.

Kinked grains were identified using an optical microscope and then mapped using the EBSD with a 2 µm step size. A match unit file for $Mg_2GeO_4$ was built using *Pnma* as the space group with $a$ = 10.304, $b$ = 6.032, $c$ = 4.913 (National Bureau of Standards Circular 539, 10, p. 38, 1960) and using the atomic positions for forsterite (Birle et al. 1968) reset into *Pnma*. After data analysis, the unit cell was recast as *Pbnm* so that the unit-cell setting is consistent with that traditionally used for olivine. Throughout this paper we use the *Pbnm* setting ($a$ = 4.913, $b$ = 10.304, $c$ = 6.032). Data from EBSD maps was analyzed using Channel 5 software. Noise reduction was performed using the routines in Channel 5's Tango program. For pole figures "wild spikes" (pixels that differ in orientation from their neighbors by

* E-mail: Burnley@physics.unlv.edu

† 🔓 Open Access: Article available to all readers via GSW (http://ammin.geoscienceworld.org) and the MSA web site.

0003-004X/13/0506–927$05.00/DOI: http://dx.doi.org/10.2138/am.2013.4224

**TABLE 1.** Conditions for the deformation experiments

| Sample no. | Temperature (K) | Pressure (GPa) | Strain rate (per s) | Total strain | Maximum stress (MPa) |
|---|---|---|---|---|---|
| GL312 | 1190(10) | 1.1 | $2 \times 10^{-4}$ | 15% | 1279(157) |
| GL265 | 990(5) | 1.4 | $2 \times 10^{-4}$ | 24% | 2481(118) |
| GL330 | 1047(5) | 1.2 | $2 \times 10^{-5}$ | 38% | 1904(197) |
| | Ramp to 1179 | 1.3 | | | |

more than 10°) were removed but no additional noise reduction was made. For the maps presented in the figures orientations were assigned to un-indexed pixels based on the surrounding 8 then 7 and 6 neighboring pixels. We have found this process to be the most effective at eliminating most un-indexed points without adding significant information to the original data. The trace of the kink band boundary on the surface of the thin section was measured with an optical microscope rather than from the EBSD orientation maps to avoid including uncertainty introduced via the image tilt correction. The orientation of kink band boundaries was determined by assuming that the kink band boundary is planar and contains both the rotation axis and the trace of the kink band boundary across the sample surface.

## RESULTS

We made detailed maps of 55 grains for this study. Twenty grains were identified as having kink bands because they contained multiple high-aspect ratio subgrains with alternating orientations. Figure 1 shows an optical micrograph, orientation image map, and pole figures for each of three of these grains. For all grains measured, the crystallographic direction that is least dispersed is the [010] direction, which we interpret to indicate that the kinks form by rotation about the [010] direction. To test this hypothesis, we constructed plots of rotation axes, in crystal coordinates for each grain containing kink bands. The plots are produced by the Channel 5 software, which calculates a misorientation angle and rotation axis that will bring each pair of measured orientation in the map into coincidence. Figure 2 shows a cumulative plot of the rotation axes, in crystal coordinates, for all the data points within the kinked grains for which the misorientation was between 10–70°. The plot shows a prominent maximum around the [010] direction. Plots of rotation axes for misorientations between 0–10° for kinked grains show a less well-developed maximum around [010] but are otherwise similar to misorientation plots for grains that do not contain kind bands. The amount of rotation around the [010] axis varies widely from one kinked grain to another and can vary substantially (up to 75°) within a single kinked grain. This variation in the degree of rotation around [010] within grains causes alternating domains with similar orientations to become progressively misoriented with respect to each other from one end of the grain to the other. This creates the dispersion of [100] and [001] directions in small circles around [010]. In misorientation transects taken perpendicular to kink band boundaries it can be seen that the misorientation between successive kink domains appears to be concentrated entirely at the kink band boundary. This is true for all kink bands, even those for which the degree of rotation between kink band domains is <10°. In misorientation transects taken parallel to the kink band boundary in the center of kink band domains, we see misorientations ranging up to 15°. Thus the degree of rotation between two kink band domains can vary significantly along the length of their mutual boundary. Kink band boundaries across which the misorientation exceedes 10° generally have some degree of cracking along the boundaries such that the kink band boundaries can be seen in plane-polarized light. Since the samples experienced pervasive microcracking

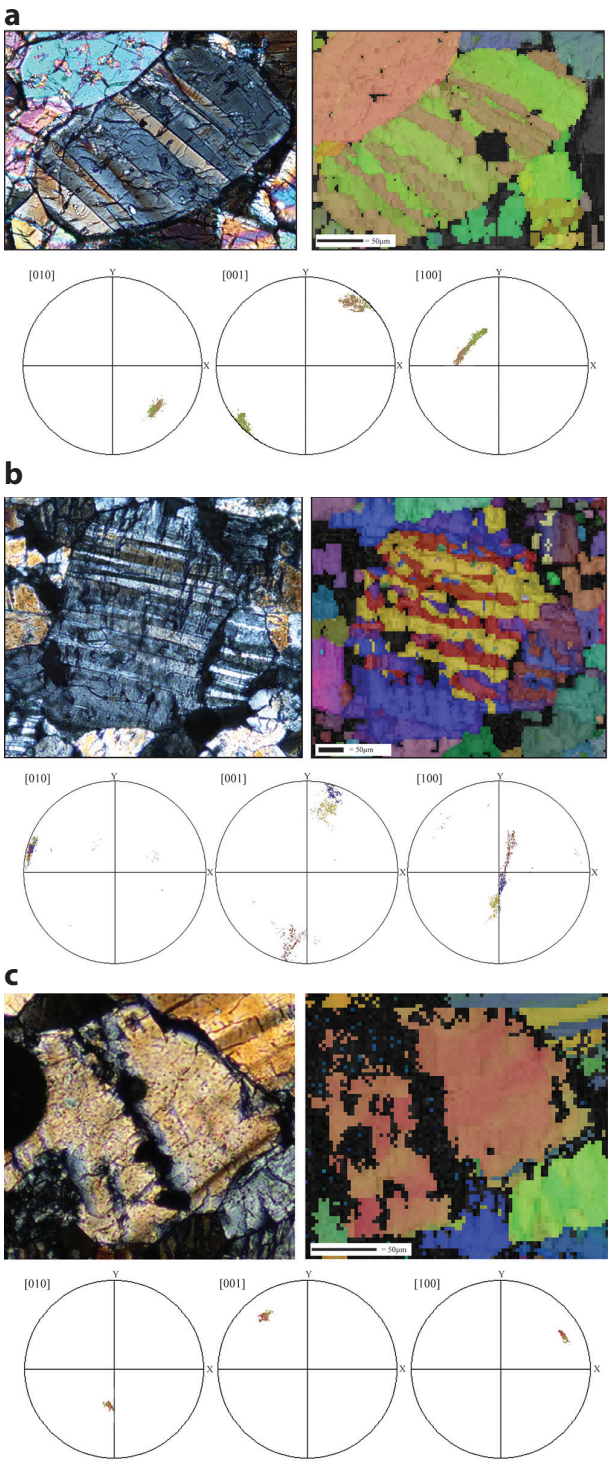


**FIGURE 1.** Orientation image maps, optical micrographs, and pole figures for three kinked olivine grains. The pole figures show the color associated with each Euler angle on the map. X is parallel to the compression direction. The group of un-indexed pixels on the right side of the kinked grain in part **a** reflects a divot in the polished surface. Un-indexed points on the right side of the kinked grain in part **b** and through the center of the kinked grain in part **c** are due to inclusions of other phases.

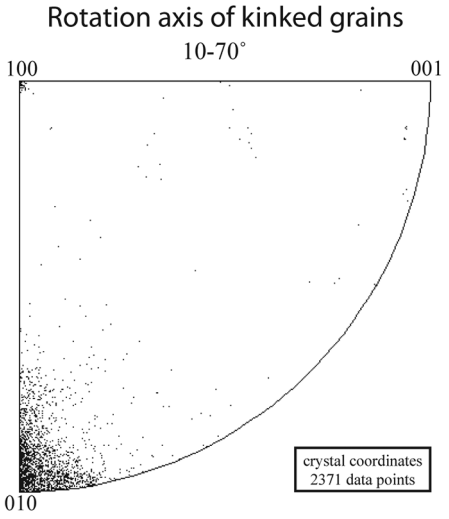


**FIGURE 2.** Inverse pole figure showing rotation axes for all orientation measurements from all kinked grains. The small cluster of rotation axes at [100] is associated with a 60° rotation about that direction is caused by systematic miss indexing.

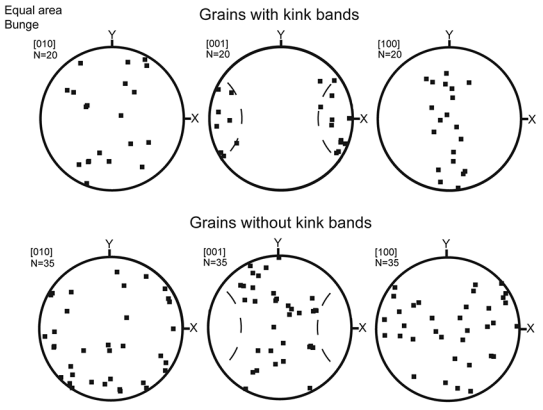


**FIGURE 3.** Pole figures showing measured orientations of grains that do not contain kink bands and reconstructed orientations (see text for explanation) of grains with kink bands. X is parallel to the compression direction. All grains that contain kinks had an original orientation that placed its [001] direction within or close to 35° of the compression direction.

during decompression, we cannot interpret the presence of the cracks in an unambiguous way. The formation of the kink bands allows the grains to shorten significantly in the direction normal to the kink band boundaries. From the misorientation angles and width of the kink bands we calculate the shortening for the grains shown in Figure 1 to be 7–8%, for some grains the shortening is as high as 15%. We reconstructed the original orientation of each kinked grain by choosing a [001] and [100] orientation that bisected the orientations observed in the kinked domains. In some cases (e.g., Fig. 1b), this orientation is preserved as a domain in the grain, usually located at the extremity of the grain. We then compared the orientation of the grains containing kink bands with the grains that did not contain kink bands (Fig. 3). We find that kinking occurs in all grains for which the angle between [001] and the compression direction is <35°. Thus we estimate that, if grains in the polycrystal are randomly oriented, 18% of all grains in these samples deformed by kinking. As mentioned above, the orientation of kink band boundaries were determined by assuming that they contain both the trace of the boundary on the sample surface and the rotation axis as determined from the misorientation plot for each grain. Since the rotation axes for all grains are parallel to the [010] direction, all the kink band boundaries lie in the [010] zone. Three quarters of the poles to kink band boundaries are within 10° of [001]; the pole with the largest deviation from the [001] direction is 22° away. From this geometry we conclude that the kink bands formed on the [001] (100) slip system.

## DISCUSSION

One of the challenges in creating numerical models of olivine deformation is that the slip systems do not satisfy the von Mises criterion for arbitrary shape change. For example, in viscoplastic self-consistent models an accommodation mechanism—or "fake" slip system must be included to close the single-crystal yield surface (Castelnau et al. 2010). The inclusion of the accommodation mechanism can have substantial impacts on the deformation models (Castelnau et al. 2010). Although it is commonly understood that kinking is an accommodation mechanism in olivine, no one has attempted to estimate its importance. Our observation that in uniaxial deformation, a significant fraction of grains not oriented for slip will kink implies that this accommodation mechanism is important and should be included in deformation models.

Kink bands were historically of interest because the geometry of kink bands can be used to unambiguously determine both the slip plane and slip direction of the slip system that forms the kinks (Raleigh 1968). The kink bands in $Mg_2GeO_4$ are visually very similar to those observed in $(Mg,Fe)_2SiO_4$ and they form in comparable conditions; those where glide dominates over recrystallization. However, the kink bands that we have characterized are of the [001] type rather than the [100] type that are most prevalent in $(Mg,Fe)_2SiO_4$. [001] type kink bands have been observed in meteorites (Carter et al. 1968) and in some experimentally deformed samples but are much less common (Raleigh 1968; Ave Lallemant 1985). In early studies, this observation was used to conclude that [100] slip is the dominant slip system operating in olivine at moderate temperature and low pressure.

Our results also appear to be in direct contradiction with the results of Vaughan and Coe (1978) who made extensive optical measurements of kink bands in experimentally deformed $Mg_2GeO_4$. For the kink bands that they measured, Vaughan and Coe (1978) found that 70% of kink bands had kink band boundaries normal to [100], 20% normal to [001], and 10% with other orientations. Their measurements were made on an optical microscope with a u-stage. This contradiction is resolved by noting that Vaughan and Coe (1978) incorrectly assigned the crystallographic axes to the optical indicatrix. Citing unpublished work by R. Erd (1977), they assigned $\alpha$, $\beta$, and $\gamma$ of the optical indicatrix to [010], [100], and [001], respectively. Both

previous (Roy and Roy 1954) as well as subsequent workers (Reichlin 1978; Weidner and Hamaya 1983) observe that β is parallel to [001] and γ is parallel to [100]. If one corrects Vaughan and Coe's work (by swapping *a* and *c*) their results and our results are consistent. Vaughan and Coe's experiments were conducted over a larger range of temperature, pressure, and differential stresses. Kinks of the [100] type were only observed at the highest temperature (1573 K) in Vaughan and Coe's study, which implies that slip in $Mg_2GeO_4$ is dominated at low to moderate temperature by [001] slip rather than [100].

### $Mg_2GeO_4$ as an olivine analog

There is an extensive literature in which various $A_2BO_4$ silicate and germanate compounds have been used as analogs for magnesium silicate olivine because these other compounds transform to the denser polymorphs at lower more experimentally accessible pressures. The assertion that we can assume that these analog phases are good analogs for mantle compositions of olivine is supported by many workers including Navrotsky (1989) who points out that the phase diagrams for many $A_2BO_4$ silicate and germanates share the same topology. The differences in phase equilibria can be explained by shifting the *PT* phase diagram for each material in topological space. $Mg_2GeO_4$ olivine and its spinel structure polymorph have been extensively used as an analog system for $(Mg,Fe)_2SiO_4$ in studies of mantle structure, phase transformation kinetics and mechanisms (Goldschmidt 1931; Bernal 1936; Jeffreys 1936; Dachille and Roy 1960; Guyot et al. 1986; Rubie and Champness 1987; Will and Lauterjung 1987; Burnley and Green 1989; Rubie and Ross 1994; Burnley et al. 1995; Burnley 1995, 2005) as well as in studies of the effect of phase transformation on the rheology of the transitions zone (Vaughan and Coe 1978, 1981; Vaughan et al. 1982, 1984; Green and Burnley 1990; Burnley et al. 1991; Tingle et al. 1993; Dupas-Bruzek et al. 1998; Riggs and Green 2001, 2005; Mecklenburgh et al. 2006). The observation that the dominant slip system is different in $Mg_2GeO_4$ could be used to call into question its fidelity as an analog system for olivine. However, it is important to keep in mind that $Mg_2GeO_4$ is a "high-pressure" analog for silicate olivine. In fact, the experiments discussed here as well as many of those conducted by Vaughan and Coe were conducted and *P-T* conditions where the olivine structure is not the thermodynamically stable phase, which is analogous to >13–14 GPa for mantle compositions of olivine. In other words, we should expect the Mg germanate lattice at low pressure to behave like the silicate lattice does at high pressure. Recently, several workers have seen evidence that the dominant slip system for mantle olivine changes from [100] to [001] at high pressure. Couvy et al. (2004) sees evidence that this shift occurs below 11 GPa and Raterron et al. (2007) sees a shift between 3 and 7.2 GPa. Using a numerical, atomistic model of dislocation core structure, Durinck et al. (2005) also finds evidence that [001] slip should become dominant at higher pressure. Their models show that slip in the [100] direction compresses the silica tetrahedra and that slip along [001] stretched the tetrahedra; thus [100] slip hardens with pressure. It makes sense then that the size difference between the $Si^{4+}$ and $Ge^{4+}$ cation should have a similar effect on the relative ease of slip as a function of pressure.

## Concluding remarks

Despite the fact that kink bands are not uncommon in naturally and experimentally deformed olivine, relatively little attention has been paid to the role of kink band formation in the deformation of olivine polycrystals over the last 30 years. Our observation that kinking occurred in all measured olivine grains oriented such that their [001] axes were within 35° of the compression direction indicates that in a randomly oriented polycrystal undergoing uniaxial deformation, 18% of all grains will deform by kinking. Thus kinking is an important accommodation mechanism in the plastic deformation of polycrystalline olivine that must be considered in models of olivine deforming by slip.

Based on the results presented here combined with the re-interpretation of the results of Vaughan and Coe (1978), which covered a wider range of conditions, we find that [001] slip is the dominant slip system operating in $Mg_2GeO_4$ olivine at 1000–1473 K at 0.6–1.3 GPa. This result is consistent with the observations made by others (Couvy et al. 2004; Durinck et al. 2005; Raterron et al. 2007) that the dominant slip system for olivine in the mantle switches from [100] to [001] as pressure increases.

## Acknowledgments

This work was supported by National Science Foundation Grants EAR94-18685 and EAR07-41521 and partially supported by DOE NNSA Cooperative Agreement No. DE FC52-06NA26274. The authors thank Sean Mulcahy for assistance with the EBSD and also thank Patrick Cordier and Florian Heidelbach for thoughtful and very helpful reviews of the manuscript. The first author thanks Harry Green for use of the experimental samples and for helpful conversations.

## References cited

Ave Lallemant, H.G. (1985) Subgrain Rotation and dynamic recrystallization of olivine, upper mantle diapirism, and extension of the basin-and-range province. Tectnophysics, 119, 89–117.

Bernal, J.D. (1936) Discussion. Observatory, London, v. 748, 267–268.

Birle, J.D., Gibbs, G.V., Moore, P.M., and Smith, J.V. (1968) Crystal structures of natural olivines. American Mineralogist, 53, 807–824.

Bjerg, E., Ntaflos, G., Kurat, G., Dobosi, G., and Labudia, C. (2005) The upper mantle beneath Patagonia, Argentina, documented by xenoliths from alkali basalts. Journal of South American Earth Sciences, 18, 2 (January), 125–145.

Burnley, P.C. (1990) The effect of nonhydrostatic stress on the olivine-spinel transformation in $Mg_2GeO_4$. Ph.D. Thesis, University of California at Davis.

——— (1995) The fate of olivine in subducting slabs: A reconnaissance study. American Mineralogist, 80, 1293–1301.

——— (2005) Investigation of the martensitic-like transformation from $Mg_2GeO_4$ olivine to its spinel structure polymorph. American Mineralogist, 90, 1315–1324.

Burnley, P.C. and Green, H.W. (1989) Stress dependence of the mechanism of the olivine-spinel transformation. Nature, 338, 753–756.

Burnley, P.C., Green, H.W., and Prior, D.J. (1991) Faulting associated with the olivine to spinel transformation in $Mg_2GeO_4$ and its implications for deep-focus earthquakes. Journal of Geophysical Research, 96, 425–443.

Burnley, P.C., Bassett, W.A., and Wu, T.C. (1995) Diamond anvil cell study of the transformation mechanism from the olivine to spinel phase in $Co_2SiO_4$, $Ni_2SiO_4$ and $Mg_2GeO_4$. Journal of Geophysical Research, 100, 17715–17723.

Carter, N.L., Raleigh, C.B., and DeCarli, P. (1968) Deformation of olivine in stoney meteorites. Journal of Geophysical Research, 73, 5439–5461.

Castelnau, O., Cordier, P., Lebensohn, R.A., Merkel, S., and Raterron, P. (2010) Microstructures and rheology of the Earth's upper mantle inferred from a multiscale approach. Comptes Rendus Physique, 11, 304–315.

Chernyshov, A. (2005) Petrostructural signature of olivine in ultramafic rocks of the paramsky and shamanskty massifs. Russian Geology and Geophysics, 46, 11, 1103–1114.

Cordier, P., Thurel, E., and Rabier, J. (2002) Stress determination in multianvil deformation experiments based on dislocation curvatures measurements: Application to wadsleyite and ringwoodite. Geophysical Research Letters, 29, 15.

Couvy, H., Frost, D., Heidelbach, F., Nyilas, K., Ungar, T., Mackwell, S., and Cordier, P. (2004) Shear deformation experiments of forsterite at 11 GPa - 1400°C in the multianvil apparatus. European Journal of Mineralogy, 16, 877–889.

Dachille, F. and Roy, R. (1960) High pressure studies of the system. $Mg_2GeO_4$-

$Mg_2SiO_4$ with special reference to the olivine-spinel transition. American Journal of Science, 258, 225–246.
Dupas-Bruzek, C., Sharp, T.G., Rubie, D.C., and Durham, W.B. (1998) Mechanisms of transformation and deformation in $Mg_{1.8}Fe_{0.2}SiO_4$ olivine and wadsleyite under non-hydrostatic stress. Physics of Earth and Planetary Interiors, 108, 33–48.
Durham, W.B. and C. Goetze. (1977) Plastic flow of oriented single crystals of olivine. 1. Mechanical Data. Journal of Geophysical Research, 82, 36, 5737–5753.
Durinck, J., Legris, A., and Cordier, P. (2005) Pressure sensitivity of olivine slip systems: First-principle calculations of generalized stacking faults. Physics and Chemistry of Minerals, 32, 646–654.
Goldschmidt, V.M. (1931) Zur kristallchemie des germaniums. Gesellschaft der Wissenschaften zu Göttingen, Mathematisch-Physikalische Klasse, Frachgr IV, Bd I., 184–190.
Green, H.W. and Burnley, P.C. (1990) The failure mechanism for deep-focus earthquakes. In R.J. Knipe and E.H. Rutter, Eds., Deformation Mechanisms, Rheology and Tectonics, 54, 133–141. Geological Society Special Publication, London.
Guyot, F., Boyer, H., Madon, M., Velde, B., and Poirier, J.P. (1986) Comparison of the Raman microprobe spectra of $(Fe,Mg)_2SiO_4$ and $Mg_2GeO_4$ with olivine and spinel structures. Physics and Chemistry of Minerals, 13, 91–95.
Jeffreys, H. (1936) The structure of the Earth down to the 20 discontinuity. Monthly Notices Royal Astronomical Society, Geophysics Supplement, 3, 401.
Kopylova, M.G., Russell, J.K., and Cookenboo, H. (1999) Petrology of peridotite and pyroxenite xenoliths from the Jericho Kimberlite: Implications for the Thermal state of the mantle beneath the Slave Craton, Northern Canada. Journal of Petrology, 40, 1, 79–104.
Low, P.C., Schultz, L., and Stier, N. (2011) Iddingzitized olivine in mantle xenoliths: Evidence for (really) early alteration. Abstract V41C-2511 presented at 2011 Fall Meeting, AGU, San Francisco, California, 5-9 Dec.
Mecklenburgh, J., Zhao, Y.-H., Heidelbach, F., and Mackwell, S. (2006) Deformation of olivine-spinel aggregates in the system $(Mg,Ni)_2GeO_4$ deformed to high strain in torsion: Implications for upper mantle anisotropy. Journal of Geophysical Research, 111, B11209, doi:10.1029/2006JB004285.
Mercier, J-C.C. and Nicolas, A. (1975) Textures and fabrics of upper-mantle peridotites as illustrated by xenoliths from basalts. Journal of Petrology, 16, 454–487.
Navrotsky, A. (1989) Silicates and germanates at high pressure. Solid State Ionics, 32, 33, 288–297.
Raleigh, C.B. (1968) Mechanisms of plastic deformation of olivine. Journal of Geophysical Research, 73, 16, 5391–5406.
Raterron, P., Chen, J., Li, L., Weidner, D., and Cordier, P. (2007) A low-temperature snowball-like process for the olivine-spinel transition. American Mineralogist, 92, 1436–1445.
Reichlin, R.L. (1978) The crystal chemistry of orthogermanates. Earth and Space Science, Master's Thesis, State University of New York, Stony Brook.
Riggs, E.M. and Green, H.W. (2001) Shear localization in transformation-induced faulting: First-order similarities to brittle shear failure. Tectonophysics 340, 1–2, 95–107.
——— (2005) A new class of microstructures which lead to transformation-induced faulting in magnesium germanate. Journal of Geophysical Research-Solid Earth, 110, B03202.
Ross, N. and Navrotsky, A. (1987) The $Mg_2GeO_4$ olivine-spinel phase transformation. Physics and Chemistry of Minerals, 14, 473–481.
Roy, D.M. and Roy, R. (1954) An experimental study of the formation and properties of synthetic serpentines and related layer silicate minerals. American Mineralogist, 39, 957–975.
Rubie, D.C. and Champness, P.E. (1987) The evolution of microstructure during the transformation of $Mg_2GeO_4$ olivine to spinel. Bulletin of Mineralogy, 110, 5, 471–480.
Rubie, D.C. and Ross, C.R.I. (1994) Kinetics of the olivine-spinel transformation in subducting lithosphere: Experimental constraints and implications for deep slab processes. Physics of the Earth and Planetary Interiors, 86, 223–241.
Tingle, T.N., Green, H.W., Scholz, C.H., and Koczynski, T.A. (1993) The rheology of faults triggered by the olivine-spinel transformation in $Mg_2GeO_4$ and its Implications for the mechanism of deep-focus earthquakes. Journal of Structural Geology, 15, 1249–1256.
Vaughan, P.J. and Coe, R.S. (1978) Geometric flow properties of the germanate analog of forsterite. Tectonophysics, 46, 187–196.
——— (1981) Creep mechanism in $Mg_2GeO_4$: Effects of a phase transition. Journal of Geophysical Research, 86, B1, 389–404.
Vaughan, P.J., Green, H.W., and Coe, R.S. (1982) Is the olivine-spinel phase transformation martensitic? Nature, 298, 357–358.
——— (1984) Anisotropic growth in the olivine-spinel transformation of $Mg_2GeO_4$ under nonhydrostatic stress. Tectonophysics, 108, 299–322.
Weidner, D.J. and Hamaya, N. (1983) Elastic properties of the olivine and spinel polymorphs of $Mg_2GeO_4$, and evaluation of elastic analogues. Physics of the Earth and Planetary Interiors, 33, 275–283.
Will, G. and Lauterjung, J. (1987) The kinetics of the pressure-induced olivine-spinel phase transition $Mg_2GeO_4$. In M.H. Manghnani and Y. Syono, Eds., High-pressure Research in Mineral Physics, 39, 177–186. Geophysical Monograph. American Geophysical Union, Washington.
Zeuch, D.H. and Green, H.W. (1984a) Experimental deformation of a synthetic dunite at high temperature and pressure. Part I. Mechanical behavior, optical microstructure and deformation mechanism. Tectonophysics, 110, 233–262.
——— (1984b) Experimental Deformation of a synthetic dunite at high temperature and pressure. Part II. Transmission electron microscopy. Tectnophysics, 110, 263–296.

Manuscript received May 9, 2012
Manuscript accepted January 24, 2013
Manuscript handled by Jennifer Kung